New insights into the degradation processes and influence of the conservation treatment in alum-treated wood from the Oseberg collection

Authors:

Caitlin M. A. McQueen[1,a], Diego Tamburini[2,a,b], Jeannette Jacqueline Lucejko[2,3], Susan Braovac[1], Francesca Gambineri[4], Hartmut Kutzke[1], Francesca Modugno[2], Maria Perla Colombini[2,3]

[1]Department of Collection Management, Museum of Cultural History, University of Oslo, Postbox 6762 St. Olavs plass, 0130 Oslo, Norway
[2] Department of Chemistry and Industrial Chemistry, University of Pisa, via Moruzzi 13, I-56124 Pisa, Italy
[3] Institute for the Conservation and Promotion of Cultural Heritage (ICVBC), National Research Council, via Madonna del Piano 10, I- 50019, Sesto Fiorentino, Florence, Italy
[4] Archa Laboratories Srl, via Tegulaia 10/A, I-56121 Pisa, Italy

Abstract
The Oseberg collection includes the most complete ensemble of wooden remains from the Viking Age. However, since many of the wooden objects were treated with alum in the early 1900s, they now suffer from dramatic conservation issues.

A multi-analytical approach was adopted to investigate both the organic and the inorganic components of some selected wood fragments, with the aim of fully characterising the materials and their decomposition products. A particular focus was on the differences between the surface and the core of the fragments analysed, and on the correlations between the results obtained by the different techniques, in order to disclose possible interactions between the materials during degradation. In addition to differences in alum concentration and wood alteration between the surface and the core, some decomposition/transformation products of alum, such as mercallite ($KHSO_4$), were identified by FTIR and XRD. Contextual interpretation of the results obtained by ICP-OES elemental analysis of inorganic components and Py(HMDS)-GC/MS characterisation of degraded lignocellulosic materials supported some previous observations about potential relationships between specific metals (Al, Fe, Ca,) and wood degradation and enabled new correlations to be highlighted.
Although similar degradation patterns were revealed in the investigated objects – depletion of holocellulose, oxidation of lignin and some transformation of alum - a notable variability at the molecular level was highlighted. This is an important factor to be taken into account for the planning of re-treatment strategies of these extremely precious artefacts.

Key words: alum, archaeological wood, degradation, potassium bisulphate, sulphuric acid, Oseberg, Py-GC/MS, XRD, IR, SEM-EDX, ICP-OES

Introduction

The Oseberg find was excavated in 1904 in Vestfold, Norway. In addition to the Oseberg ship and a number of metal artefacts and textiles, a collection of wooden objects was found, comprising a

[a] These authors contributed equally to this work.
[b] Present address: Department of Scientific Research, The British Museum, Great Russell Street, London WC1B 3DG

ceremonial wagon, three sleds, and animal head posts which lay together with cooking kits, weaving tools and looms, agricultural implements and ship gear. The burial, dated to 834 AD, was made for two women of high standing [1]. For the first time, the contents of the grave provided archaeologists and art historians with insight into Viking Age burial rituals, the types of objects that were used as a part of everyday life, as well as Viking Age wood-working technology and wood-carving achievements [2]. Part of the find is exhibited at the Viking Ship Museum in Oslo, Norway.

Today most of the objects that were treated with alum ($KAl(SO_4)_2 \cdot 12H_2O$) after excavation suffer from extreme deterioration, compromising the structural integrity of the wood. The ceremonial sleds, parts of the wagon and hundreds of other objects underwent this treatment. In the worst cases the wood has become powder. The degradation has been linked to the alum conservation treatment applied over one hundred years ago [3]. The alum treatment – as it was used on the most degraded wood from the Oseberg finds – involved soaking the waterlogged fragments in hot (90^0C) concentrated solutions of alum for up to 36 hours, in order to prevent shrinkage during drying [2]. As alum did not fully penetrate the wood during treatment, two zones were created in fragments greater than 1 cm in thickness and 10 cm in length: a hard alum-rich surface (≈ 5mm thick, across the wood grain) surrounding a much softer alum-poor core. This uneven salt distribution has influenced both mechanical and chemical properties.

The mechanisms behind the observed chemical deterioration are complex and difficult to fully elucidate. However, the release of sulphuric acid during alum treatment is believed be a key factor in their current, mechanically weakened state [3]. The wood is at present highly acidic (pH ≤ 2). Previous analyses have found that the carbohydrate component of wood is almost completely absent, and that lignin has undergone an extreme level of oxidation [4]. Additionally, correlations observed between Fe and Ca concentrations and wood degradation have suggested that the presence of these ions could be involved in the degradation pathways [4]. However, many questions remain about the particular degradation of these objects and the roles and interactions between the various materials present.

Problems with metal compounds, in particular those containing iron, and sulphuric acid in archaeological waterlogged wood have been documented in well-known case studies on shipwrecks such as the Vasa, Mary Rose and Batavia [5-8]. Fundamental research carried out in these case studies has provided valuable information about degradation processes occurring in marine archaeological wood [8-12], as well as the problems associated with their conservation [7, 13, 14]. However, significant differences between the case studies described in the literature and the Oseberg collection can be highlighted: although the Oseberg collection was discovered in waterlogged condition, it was not found in a marine environment, and the collection was notably treated with alum, rather than polyethylene glycol (PEG), which has been commonly used for waterlogged wood since the 1960s [15]. The sulphuric acid therefore arises from the sulphates introduced in the alum treatment, rather than by oxidation of reduced sulphur species accumulated in a marine environment. Moreover, the extent of the degradation is particularly dramatic, and chemical influences other than sulphuric acid may have played a significant role [4]. The alum-treated Oseberg finds also represent a class of objects found in many collections – especially in Scandinavia – which were conserved by what is today an obsolete method. The consequences of this treatment method have only recently received research focus and require dedicated investigations to increase our understanding of this type of archaeological wood.

We have previously reported initial studies into the chemical composition of wood from the Oseberg collection and decomposition of alum [3, 4]. We herein expand on this work using a wider range of analytical techniques including X-ray tomographic microscopy, SEM-EDX, FTIR, X-ray diffraction (XRD), inductively coupled plasma-optical emission spectroscopy (ICP-OES), ionic-conductivity liquid-chromatography (IC-LC) and analytical pyrolysis coupled with gas chromatography and mass spectrometry with *in situ* silylation using hexamethyldisilazane

(Py(HMDS)-GC/MS). In addition to better characterising previously studied wood fragments, we have included samples from larger pieces in which uneven alum distribution is more apparent. Our aims here are to highlight the differences in the chemical composition between the alum-rich surface and the alum-poor core of the wood fragments, characterise the minor decomposition products and understand the role of the various components in wood degradation. This knowledge will contribute to the ongoing development of retreatment strategies for the long-term preservation of the artefacts.

Materials and methods

Samples

Archaeological wood samples comprised of fragments from two different unreconstructed objects from the Oseberg find which had been treated with alum but not with any other materials. Their extreme deterioration made it difficult to identify the wood species used, though examination at lower magnification indicated that they are made of a diffuse porous hardwood, very likely birch (*Betula sp*.), based on identification of fragments from other objects. Alum (Merck, pro analysis grade) was analysed as a reference for FTIR, ICP-OES and IC-LC analyses. Sound birch was used as reference sample for FTIR and Py(HMDS)-GC/MS analyses.

Eight samples were taken from four large alum-treated fragments from a simple sled, here named the 229 fragments: 5, 1B, 1C and 1D (Figure 1a). For each fragment from 229 the samples were taken from two regions: alum-rich (AR), close to the surface and alum-poor (AP), from the core. The samples were thus named using the fragment number and then AP or AR, depending on the region they were taken from (e.g. sample 1B-AP = sample taken from the alum-poor, core, of fragment 1B). Infrared spectra for these fragments included alum salts as they were found in the sample.

Additionally, six alum-treated fragments from a loom, which originally fit together, are referred to as the 185 series (labelled 185-1 to -6, Figure 1b). As they are small, they do not have distinct alum-rich and -poor zones, and may be considered as alum-rich. Samples from these were previously described and characterised by Py(HMDS)-GC/MS and ICP-OES analyses [4]. Here they have been analysed with supplementary techniques (X-ray tomographic microscopy, SEM-EDX and FTIR and XRD) to broaden our understanding of the chemistry of alum-treated wood. For these fragments, infrared spectroscopy was performed after rinsing samples of alum salts using distilled water and air drying.

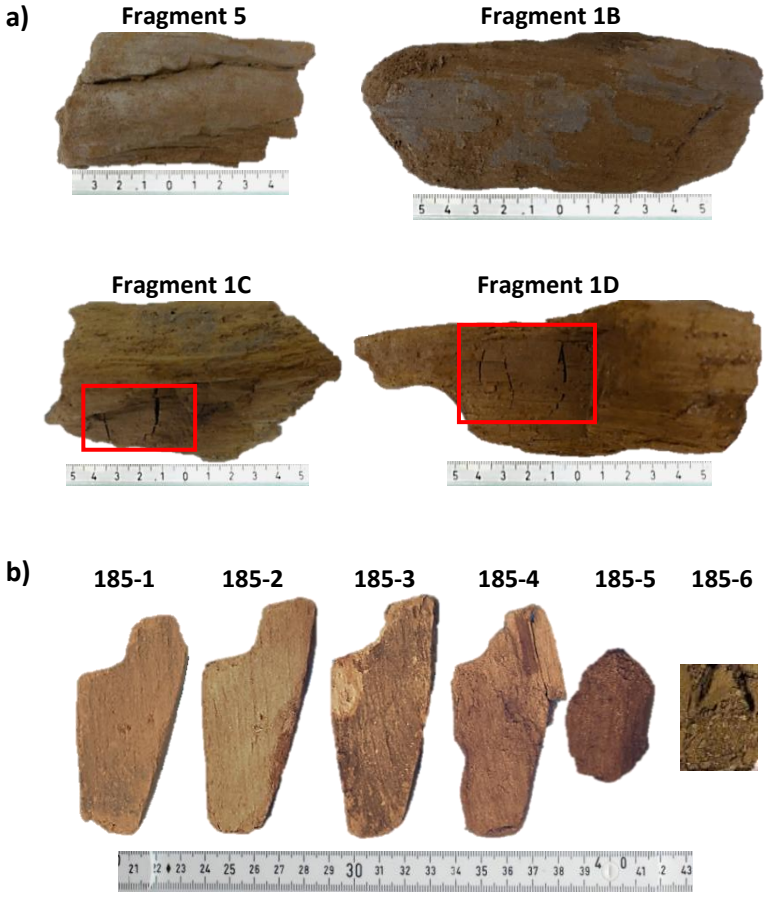

Figure 1: Alum-treated fragments from (a) a simple sled, named the 229 fragments. 229 fragments 1C and 1D have been broken since their conservation with alum, exposing the inner wood (alum-poor region), often showing internal cracks formed upon drying (red squares); (b) a loom, named the 185 series.

Instrumentation

X ray tomographic microscopy

Tomographic images were obtained from the TOMCAT beamline located at the Swiss Light Source synchrotron facilities, Paul Scherrer Institute. The X ray energy used was 18 keV at 400 mAmp, and 1500 projections were recorded. Images were captured by a CCD camera with scintillation foil. Projections were reconstructed using the software VG Studio Max 2.1, Volume Graphics, Heidelberg, Germany.

SEM-EDX

A JEOL JSM-840 scanning electron microscope was used. Cross sections of the samples were sputtered using carbon before observation. The accelerating voltage was 20 keV and the electron source was a tungsten filament.

Infrared spectroscopy

FTIR spectra in ATR mode were recorded on a Thermo Scientific Nicolet iS50 spectrometer equipped with a diamond crystal and DTGS detector. Each spectrum was recorded with 256 scans at 4 cm^{-1} resolution, within the range 4000-400 cm^{-1}. All the samples were analysed in triplicate and spectra were subsequently averaged using OMNIC32 software (Nicolet Instrument Corporation, USA).

Some spot analyses and mapping were performed both with conventional IR radiation (using the above instrument), and synchrotron radiation (SR). SR-FTIR, which gave improved spatial resolution, was carried out at the IRIS beamline at the BESSY II synchrotron facility, Helmholtz-Zentrum Berlin Germany, using a Nicolet Nexus 870 spectrometer. Samples were compressed in a diamond cell and micro-infrared spectroscopy (µFTIR) performed using a Nicolet Continuum FTIR microscope. Spectra were recorded in transmittance mode with a spectral resolution of 4 cm^{-1}, within the range 4000-650 cm^{-1} and 4000-800 cm^{-1} for conventional and synchrotron radiation, respectively. Each spectrum in the maps was recorded with 128 scans and spot analyses were recorded with 256 scans.

Py(HMDS)-GC/MS

Analytical pyrolysis was performed using 1,1,1,3,3,3-hexamethyldisilazane (HMDS, chemical purity 99.9%, Sigma Aldrich Inc., USA) as a silylation agent for the *in situ* thermally assisted derivatisation of pyrolysis products. The instrumentation consisted of a micro-furnace Multi-Shot Pyrolyzer EGA/Py-3030D (Frontier Lab) coupled to a gas chromatograph 6890 Agilent Technologies (USA) equipped with an HP-5MS fused silica capillary column (stationary phase 5 % diphenyl – 95 % dimethyl-polysiloxane, 30 m x 0.25 mm i.d., Hewlett Packard, USA) and with a deactivated silica pre-column (2 m x 0.32 mm i.d., Agilent J&W, USA). The GC was coupled with an Agilent 5973 Mass Selective Detector operating in electron impact mode (EI) at 70 eV. The pyrolysis temperature was 550 °C and interface temperature was 250 °C. Approximately 100 µg of sample and 5 µL HMDS were inserted into the platinum cup. Before analysis, all the samples were oven-dried for 24 h at 40-50 °C to remove residual water (alum salts were not removed). Samples were analysed in triplicate. Details about analytical conditions, identification of compounds and determination of relative amount of wood components are presented in [4].

ICP-OES and IC-LC

A specific analytical protocol was applied for the sample treatment. Each sample was divided into two sub-samples: one sub-sample was subjected to elemental analysis by ICP-OES. The other sub-sample was extracted in water at 60°C for 30 minutes, using ultrasound (US). Then, the eluate was analysed by IC-LC to detect anions.

For ICP-OES analyses, after micro-wave assisted mineralisation of the samples using HNO_3 65%: H_2O_2 10% (4:1), the concentration of various elements including Al, Ca, Fe, K, and S were measured. The instrument was an Optima 5300 DV, Perkin-Elmer. Elements were quantified on a 5-point calibration curve in concentrations ranging from 50 to 5000 µg/L. Sulphur was quantified on a 5-point calibration curve from 100 to 10000 µg/L.

For IC-LC analyses, the water extracts were filtered through a cellulose nitrate membrane of 0.45 µm pore size. Anions were determined using a Dionex ICS-1000 (Thermo Scientific). The concentrations of sulphates were obtained from a 5-point calibration curve in the concentration range from 1 to 10 mg/L.

XRD

X-ray diffraction analysis was carried out using a PANalytical diffractometer Empyrean Series 2 with radiation CuKα1 =1.54 Å, operating at 45 kV, 40 mA, 2θ range 5–80° step size 0.03°, time per step 5000 s, rotation time 2.0 s, equipped with a PIXcel^{1D}-Medipix3 RTMS detector, and High Score data acquisition and interpretation software. A zero background sample holder was used. Crystalline phases were identified using the ICDD database.

Results

Morphological investigations

X-ray tomographic microscopy was undertaken on samples from the 185-series (except for 185-6, as it was too degraded) in order to investigate the distribution of alum in the wood at the cellular level. The reconstructed image of 185-1 (Figure 2) clearly shows the inhomogeneous distribution of alum salts (light spots) in both vessels and fibres in the alum-rich zone. This inhomogeneity was also observed in the other samples and can thus be considered to be 'typical' of alum-treated wood in general.

Unlike X-ray tomography, SEM images did not show alum distribution as clearly, as it is a surface imaging technique, but also because it was impossible to prepare polished surfaces, due to their high level of deterioration. Nonetheless, SEM allowed us to study morphology at higher magnifications. Figure 3 shows SEM images at 250x and 1500x magnifications for samples 1D-AP and 1D-AR, which are representative for all alum treated samples discussed here (both 229 and 185 fragments). The cell walls are significantly thinner with respect to sound wood. The middle lamella is the only part of the cell wall that has survived, but it too shows signs of degradation, most notably in the regions of delamination from neighbouring cells. The observed degradation explains the extreme mechanical weakness of the cellular structure. The uneven penetration of alum has resulted in some deformation of cell walls during drying. More alum was evident in the alum-rich samples than in alum-poor samples (see also Figure 7 mapping of Al, S, K).

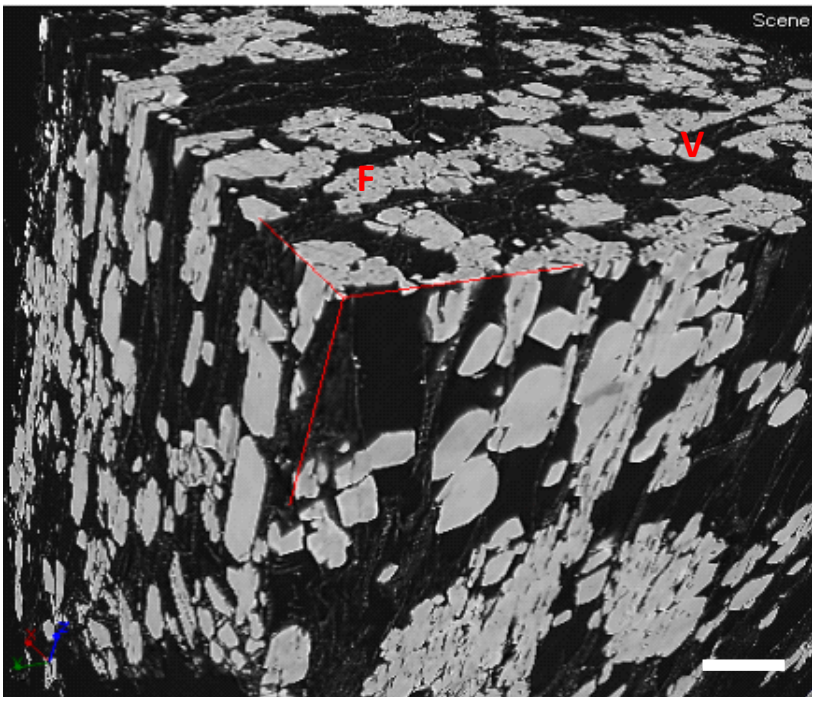

Figure 2: Sample 185-1 (alum-rich), after 3D-reconstruction from X-ray micro-tomography data. Alum salts have been deposited in both vessels (V) and fibres (F). Bar shows 50 µm.

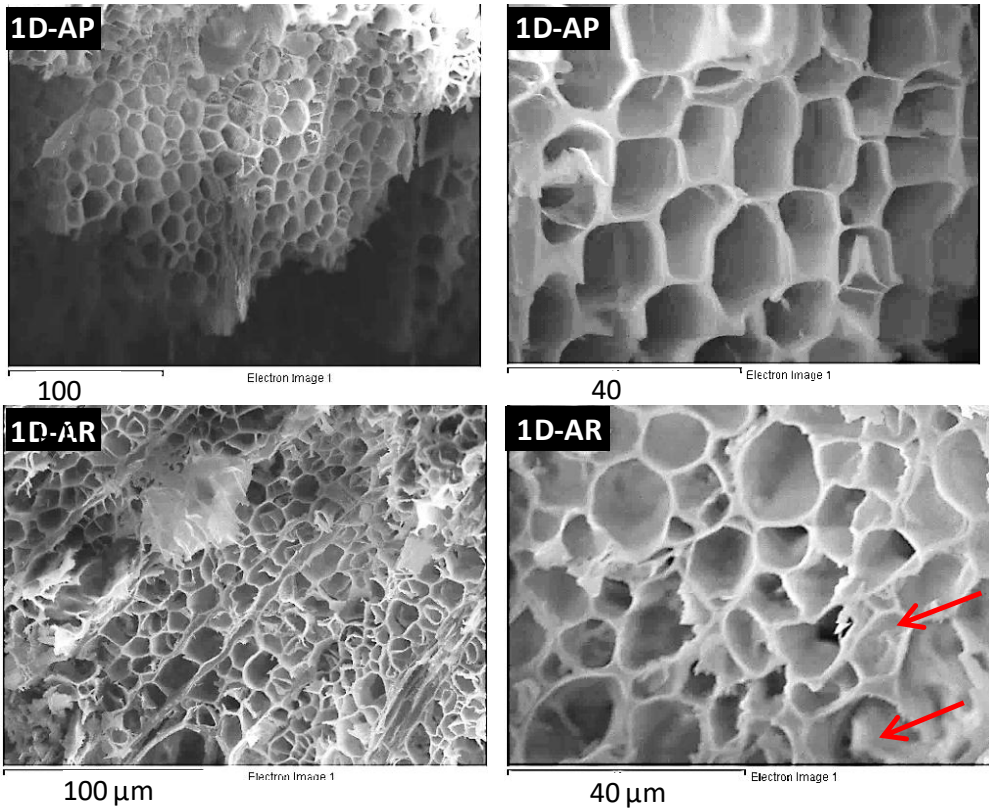

Figure 3: SEM images showing transverse sections of Fragment 1D of alum-poor (AP) and alum-rich (AR) regions. Red arrows indicate alum inside some of the wood cells.

Analyses of organic components

Infrared spectroscopy

Figure 4a shows the region 1850-400 cm^{-1} of averaged spectra from the alum-poor zones in the 229 fragments, and references of alum salt and sound birch wood; Figure 4b shows spectra from the alum-free 185 series.

In sound birch, most bands have contributions from all wood polymers (cellulose, hemicelluloses and lignin); only a few bands are purely attributed to carbohydrates or lignin [16-18]. The band at 1505 cm^{-1} arises purely due to aromatic skeletal vibration (C=C) in lignin [16, 18]. The presence of the band at 897 cm^{-1}, assigned to C-H deformation of cellulose and the band at 1156 cm^{-1}, assigned to C-O-C asymmetric valence vibration of both cellulose and hemicelluloses (which together are termed holocellulose) indicate the presence of these structural polymers. The band at 1371 cm^{-1}, assigned to C-H bending is characteristic of cellulose, whereas the band at 1736 cm^{-1}, assigned to C=O stretching in unconjugated ketones, carboxyl and ester groups derived mainly from hemicelluloses. The broad band between 1100 and 900 cm^{-1} and that at 1235 cm^{-1} are attributed to combination bands, containing signals from both holocellulose and lignin [16, 17].

As regards alum, there is a slight overlap with wood spectra at 1615 cm^{-1}, from the water of crystallisation [19, 20] and a strong overlap between 1215 and 875 cm^{-1} attributed to stretching modes of the sulphate group [21], which complicate spectral interpretation for alum-treated samples. In fact, the FTIR spectra obtained for all alum-rich samples (not shown) demonstrated strong overlapping of the alum signals with those from wood, indicating a high concentration of alum. The spectrum of Fragment 1B-AP is also heavily influenced by alum salts, indicating that

there was not a clear distinction in alum-rich and alum-poor zones for this fragment. This fragment was smaller than the others, so it follows that the alum-rich and alum-poor regions may not have been as distinct as in the larger fragments. Even though alum signals still interfere to some degree in spectra from the alum-poor samples, signals for wood are more prominent, and are thus considered in more detail below.

Aside from Fragment 1B-AP, it was possible to elucidate deterioration trends in the remaining alum-poor samples, especially between 1750 and 975 cm^{-1}. The bands assigned to cellulose and hemicelluloses (1736, 1371 and 1235 cm^{-1}) were mostly absent. Other bands emerged due to holocellulose degradation, such as that at 1113 cm^{-1} (C–H in-plane deformation in lignin) on the edge of the broad band at 1030 cm^{-1} [17, 18, 22, 23]. The alum-treated samples also showed a broad band at around 1700 cm^{-1} corresponding to stretching C=O from carboxylic acids, and conjugated aldehydes and ketones [24], indicating oxidation products had formed in the remaining lignin. Generally, the enhancement of signals from lignin occurs across the entire fingerprint region.

Spectra from the 185 series in Figure 4b also mainly show signals from lignin, but which are more prominent than those from the alum-poor samples, as the alum has been rinsed away before analysis. For instance, the bands at 1265 and 1225 cm^{-1} (assigned to the C-O stretch in the guaiacyl ring [22] and to C-O stretch of the syringyl ring [23], respectively) are now possible to discern. These lignin bands emerged due to a reduction of the signal at 1235 cm^{-1} as a result of hemicellulose degradation. It is also possible to observe increasing oxidation at 1705 cm^{-1} progressing from 185-1 to 185-6, which agrees well with the increasing visual deterioration of these samples, noted by the fragments' increasing darkness and decreasing structural integrity.

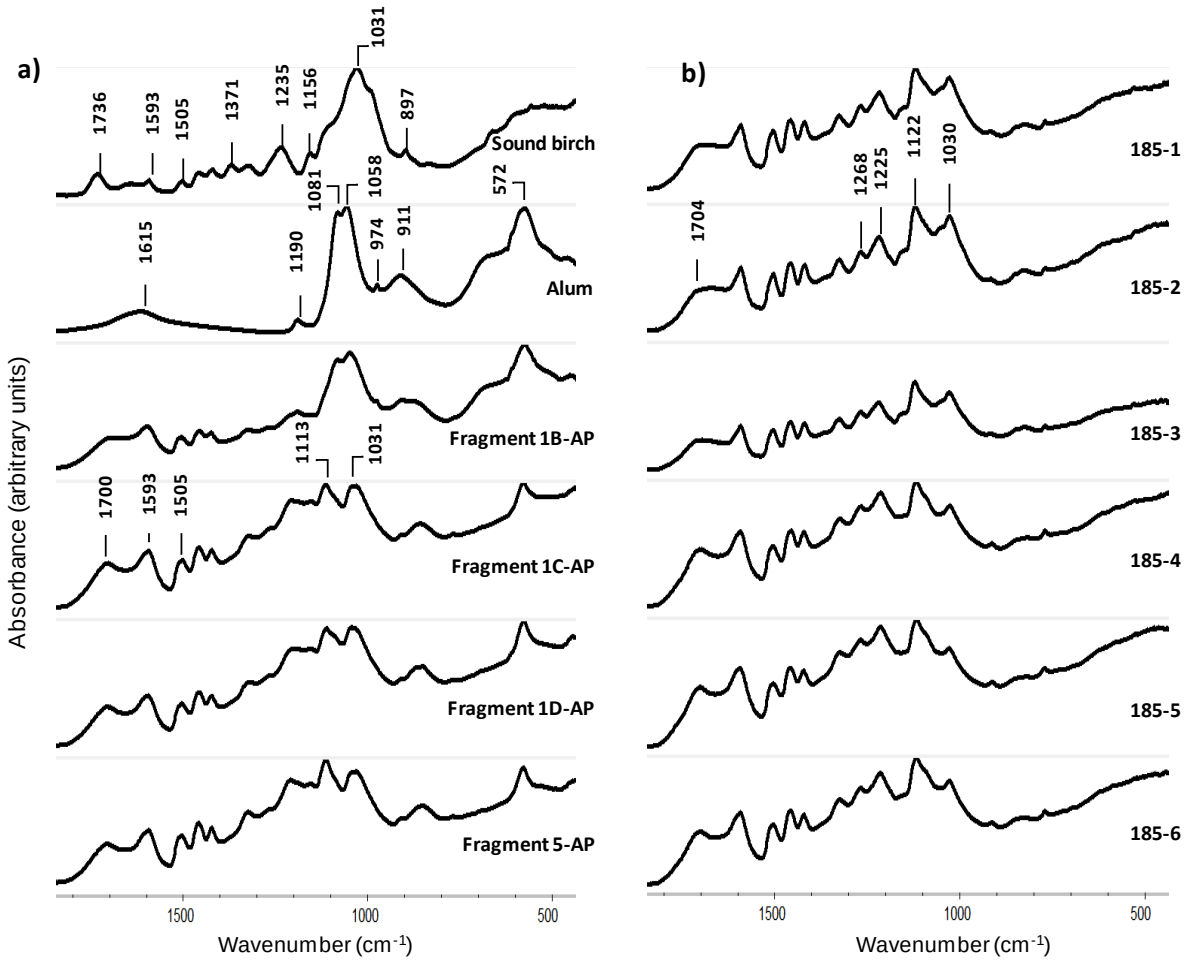

Figure 4: The fingerprint region for (a) references for sound birch and alum salt shown with spectra from the alum-poor zone in Oseberg's '229' fragments. The spectrum of Fragment 1B-AP is heavily influenced by alum salts, indicating that there was not a clear distinction in alum-rich and alum-poor zones for this fragment; (b) the 185-series, after rinsing out alum salts.

Py(HMDS)-GC/MS

Pyrolytic profiles showed remarkable differences between sound birch and the alum-treated archaeological wood. Figure 5 shows the profiles obtained for samples 1C-AP, 1C-AR and for sound birch. Although the pyrograms for AP and AR samples taken from the same fragments appear qualitatively very similar, they differ in proportions of lignin pyrolysis products, as discussed in greater detail below.

Dividing the sums of chromatographic peak areas from both holocellulose (H) and lignin (L) enables the pyrolytic H/L ratio to be obtained, which is generally used to indicate extent of degradation of holocellulose, as it is more easily broken down than lignin. H/L ratios were very low for the archaeological samples (<0.10), while that for sound birch was 3.1. This demonstrates an almost complete loss of holocellulose in the alum-treated samples, with only 2-8% abundance remaining. For sound birch, holocellulose-derived pyrolysis products made up *ca.* 75% of total abundance, of which *E*-2,3-dihydroxycyclopent-2-enone and 1,6-anhydro-β-D-glucopyranose (levoglucosan) dominated the holocellulose fraction. This was in agreement with the results obtained by FTIR as well as with pyrolysis results previously obtained for the extremely degraded woods from the 185 series [4].

As lignin is the major polymer remaining in the samples, lignin-derived pyrolysis products were examined in greater detail by sorting them into six categories [25]: monomers (intact lignin units of coniferyl and sinapyl alcohols), long chain (compounds with three carbons in the side chain, but modified compared to the monomers), short chain (compounds with side chains up to two carbon atoms), demethylated/demethyoxylated (compounds in which methyl or methoxyl groups are removed from the aromatic ring), carbonyl (compounds containing aldehyde and ketone functionalities), and acid (compounds containing carboxyl functionalities). The percentage abundances of each category with respect to total lignin content were calculated for the samples from the 229 fragments and the results shown in Figure 6.

Monomers and long chain lignin pyrolysis products generally showed very low relative abundances with respect to sound birch, indicating an almost complete fragmentation of lignin propanoid side chains and implying its extensive depolymerisation. The relative abundances of acid lignin pyrolysis products were particularly high (40-80%) in the alum-treated samples (Figure 6) indicating extensive lignin oxidation. The predominant acids identified were vanillic and syringic acids. For all fragments, lignin oxidation was higher in AR samples than in the corresponding AP samples. Both alum-poor and alum-rich samples from fragment 1B showed the highest relative abundance of acidic lignin pyrolysis products and they were the only samples containing *p*-hydroxybenzoic acid (*ca.* 10%). The presence of *p*-hydroxybenzoic acid indicates an advanced stage of lignin oxidation, showing that this sample is in the worst state of chemical preservation of the set investigated here. Its extensive chemical degradation is also reflected in what we can visually observe, as this fragment is very dark and more crumbly than the others (Figure 1). Fragment 1D-AP showed higher relative abundances of demethylated and short chain pyrolysis products, suggesting that oxidation reactions were less advanced in this fragment with respect to the others. The high levels of oxidised lignin also corresponded with the enhancement of carbonyl and carboxyl signals detected in alum-treated woods by FTIR.

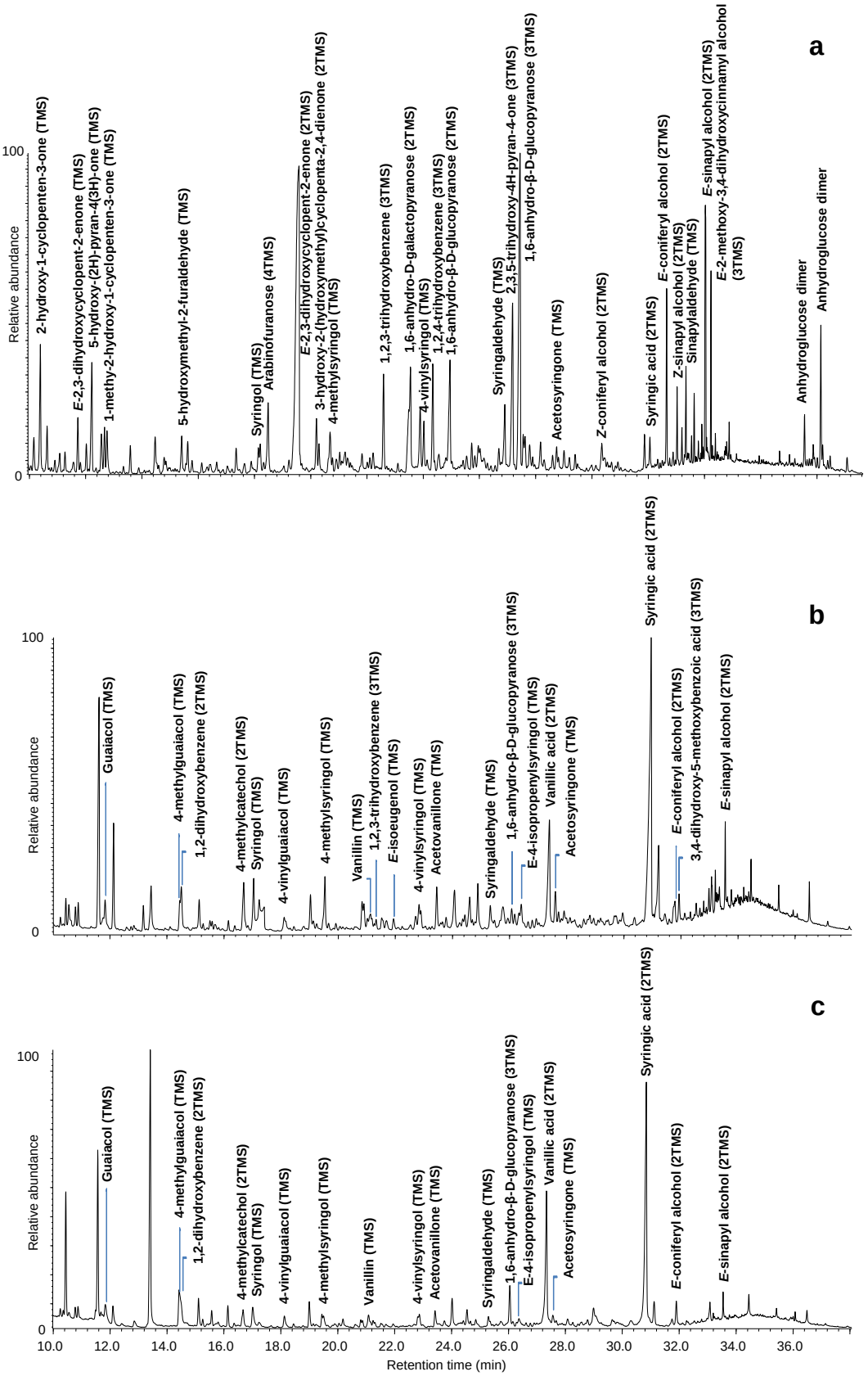

Figure 5: Py(HMDS)-GC/MS chromatographic profiles of (a) reference sound birch wood, (b) sample 1C-AP and **c)** sample 1C-AR. The Identification of pyrolysis products is based on [4].

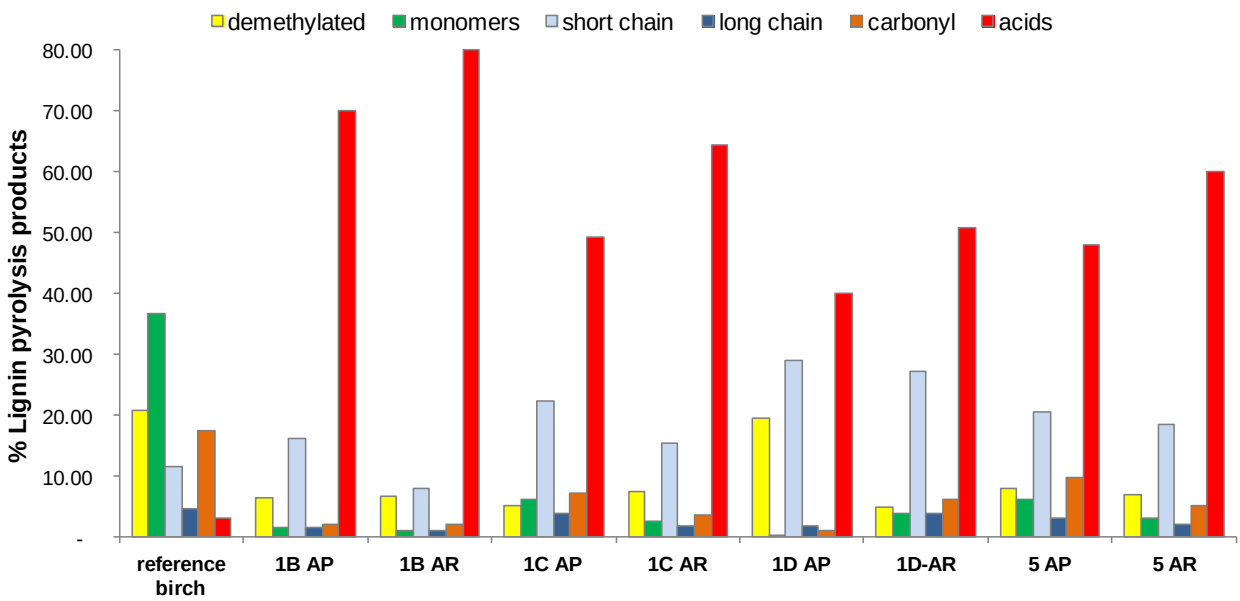

Figure 6: Relative abundances of lignin pyrolysis products grouped into categories, expressed as percentages.

Analyses of inorganic components

SEM-EDX

SEM-EDX was used to investigate the distribution of single elements from alum - Al, K and S - on samples 185-1, 185-6 and 229 fragments 1C and 1D. In Figure 7 elemental maps obtained for alum-poor and alum-rich samples from fragment 1D are shown. The 229 AP samples generally showed an even distribution of K and S at 250x magnification. Some intense spots were noticed in the K mapping, whose position corresponded to intense spots in the S mapping (Figure 7a). Although likely present in small amounts in alum-poor zones, Al was not detected, probably due to the low sensitivity of this technique to lighter elements in small concentrations. However, analyses clearly indicated significant differences in concentration of Al, K and S. Similarly, low to undetectable levels of Al were observed in 185-6, while the abundance of K and S was quite high (not shown). Hutchings [26] found similar differences between Al and the other elements using SEM-EDX on Oseberg wood.

The 229 AR samples (Figure 7b) and 185-1 (not shown) mainly showed the co-presence of Al, K and S in vessels, indicating the preferential deposition of alum salts in larger pores (see Figure 2). Nevertheless, S seemed to be more widely distributed than Al and K, indicating the presence of compounds other than alum.

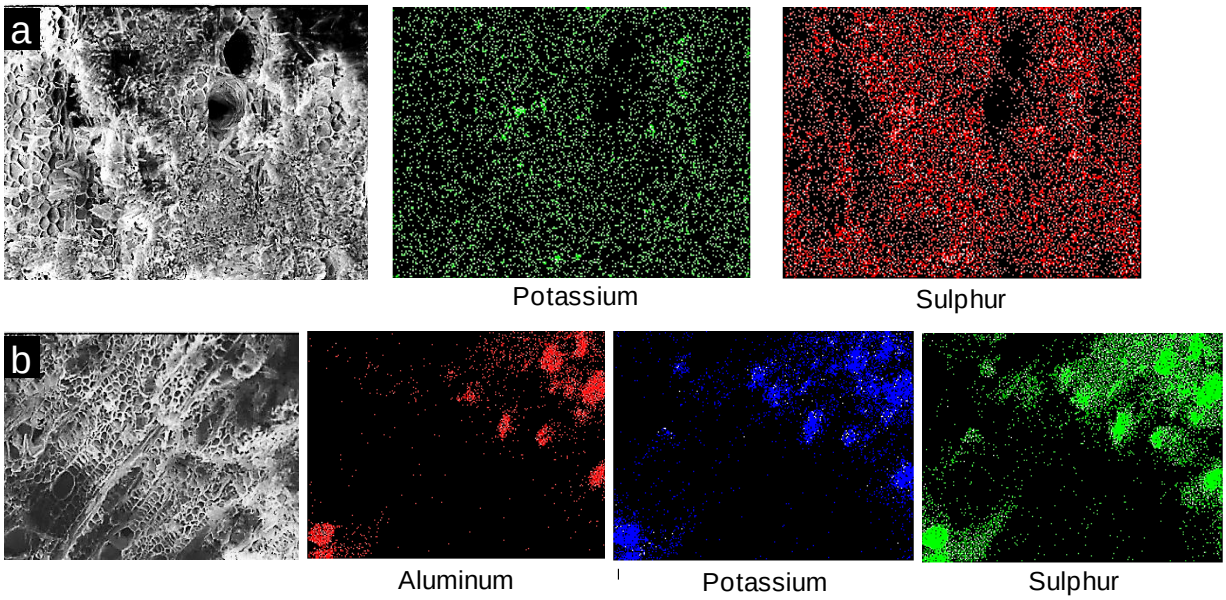

Figure 7: EDX elemental maps for a) sample 1D-AP and b) sample 1D-AR at 250x magnification.

ICP and IC-LC results

Previous ICP analysis of the 185 series samples yielded some interesting results [4]. ICP-OES analysis was therefore also obtained for the 229 fragments, and selected elements are shown in Table 1, as well as IC-LC data for sulphate concentrations in eluates from water extraction of the samples.

Table 1: ICP-OES and IC-LC results for the Oseberg samples and alum reference expressed as mmol/100g.

ICP-OES	**Alum**	**1B-AP**	**1B-AR**	**1C-AP**	**1C-AR**	**1D-AP**	**1D-AR**	**5-AP**	**5-AR**
Al	230.3	194.8	198.1	25.3	179.8	16.6	105.2	67.9	153.2
Ca	0.1	0.6	1.0	3.6	1.4	2.5	3.5	2.4	2.1
Fe	0.1	0.7	2.4	1.1	2.9	1.2	2.7	1.1	3.5
K	184.7	167.9	183.1	63.9	184.1	53.9	141.7	83.1	188.9
S	418.0	610.0	653.0	247.9	618.3	170.3	429.5	289.6	599.7
Al/K	*1.2*	*1.2*	*1.1*	*0.4*	*1.0*	*0.3*	*0.7*	*0.8*	*0.8*
Al/S	*0.6*	*0.3*	*0.3*	*0.1*	*0.3*	*0.1*	*0.2*	*0.2*	*0.3*
K/S	*0.4*	*0.3*	*0.3*	*0.3*	*0.3*	*0.3*	*0.3*	*0.3*	*0.3*
IC-LC	**Alum**	**1B-AP**	**1B-AR**	**1C-AP**	**1C-AR**	**1D-AP**	**1D-AR**	**5-AP**	**5-AR**
SO_4^{2-}	626.5	590.8	600.0	370.2	656.5	228.8	582.0	311.9	589.5

The results highlighted the difference between alum-poor and alum-rich regions in terms of different concentrations of alum elements: aluminium, potassium and sulphur. These were considerably higher in alum-rich regions than alum-poor, as expected, except for fragment 1B, which showed similar concentrations of the major elements in both regions. Iron concentrations were higher in AR than in AP samples, whereas calcium concentrations did not seem to follow an exact trend. The IC analyses also showed higher concentrations of sulphates in AR than AP samples, with the exception of samples from fragment 1B. The similarities between samples 1B-AP and 1B-AR were also reflected in the FTIR and pyrolysis results.

In order to evaluate the stoichiometric ratios between the major elements Al, K and S the ratios between Al/K, Al/S and K/S were calculated (Table 1). In AR samples, as well as in both samples from fragment 1B and fragment 5, the ratios between Al and K were close to 1, as they would be according to the alum formula ($KAl(SO_4)_2 \cdot 12H_2O$). The Al/K and Al/S ratios for samples 1C-AP and 1D-AP were significantly lower than in the AR samples, confirming the uneven distribution of Al ions highlighted by SEM-EDX. Al/S and K/S ratios were all 0.3 or below, consistently lower than the values for alum. This suggested that a substantial proportion of the sulphur in these samples is not present in the form of alum, or other potassium-containing sulphates. Nevertheless, the concentration of S in the wood samples found by ICP-OES and the concentration of sulphates in the water extract found by IC-LC analysis were generally in good agreement. Although a direct comparison of these two results is not scientifically correct, as two different techniques were used and the samples underwent different preparation, such good agreements most likely indicate that most of the sulphur was indeed present in the sulphate/sulphuric acid form.

XRD

XRD investigations identified alum and mercallite ($KHSO_4$) in almost all samples from both the 185 series and 229 fragments. No K_2SO_4 was clearly observed, indicating that the by-products of alum decomposition preferentially crystallise as the bisulphate, which is unsurprising given the low pH of these samples.

For samples 1C-AP and ID-AP, the peaks for mercallite are noticeably more intense than in the other samples, relative to the alum peaks. Figure 8 compares the diffraction patterns from samples 1C-AR and 1C-AP and a reference pattern for mercallite.

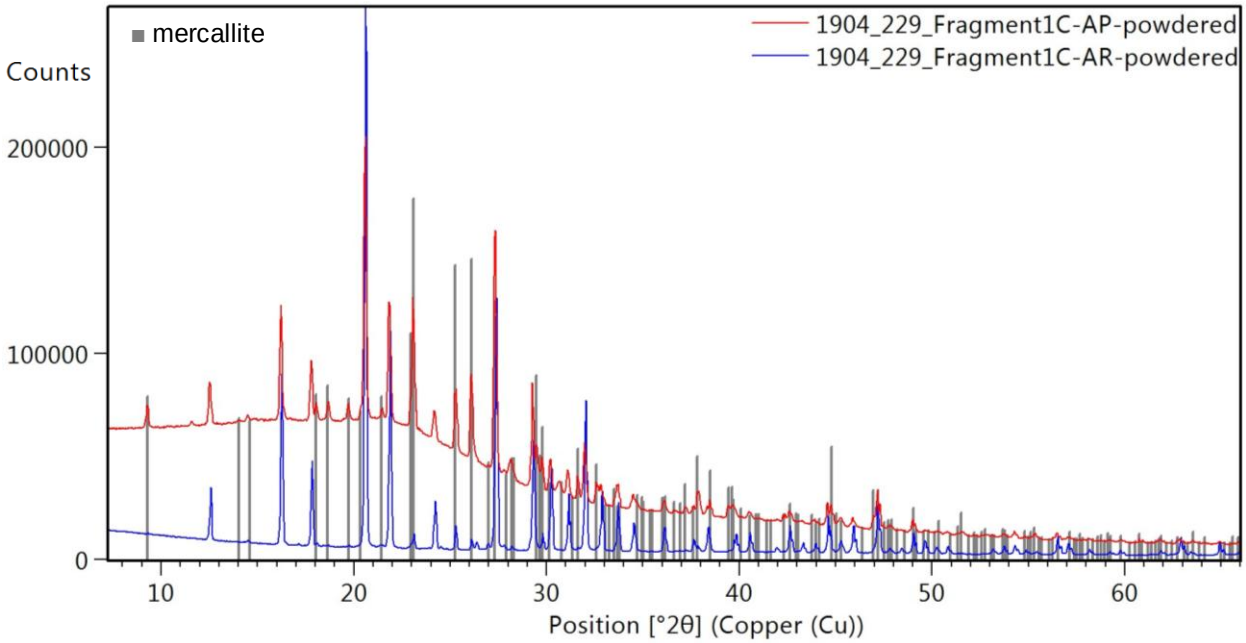

Figure 8: X-ray diffraction pattern obtained for Fragment 1C AR and AP and mercallite reference

Additionally, in all patterns of the AP samples, except 1B-AP, a broad hump in the baseline indicated the presence of an amorphous component. Figure 9 compares the diffraction pattern of 1D-AP with that of 185-2 after rinsing out alum. It can be seen that the location of the baseline humps are similar, indicating that the amorphous phase detected in the alum poor samples is likely from the wood component, which is not seen in the more alum rich samples due to the higher alum-to-wood ratio.

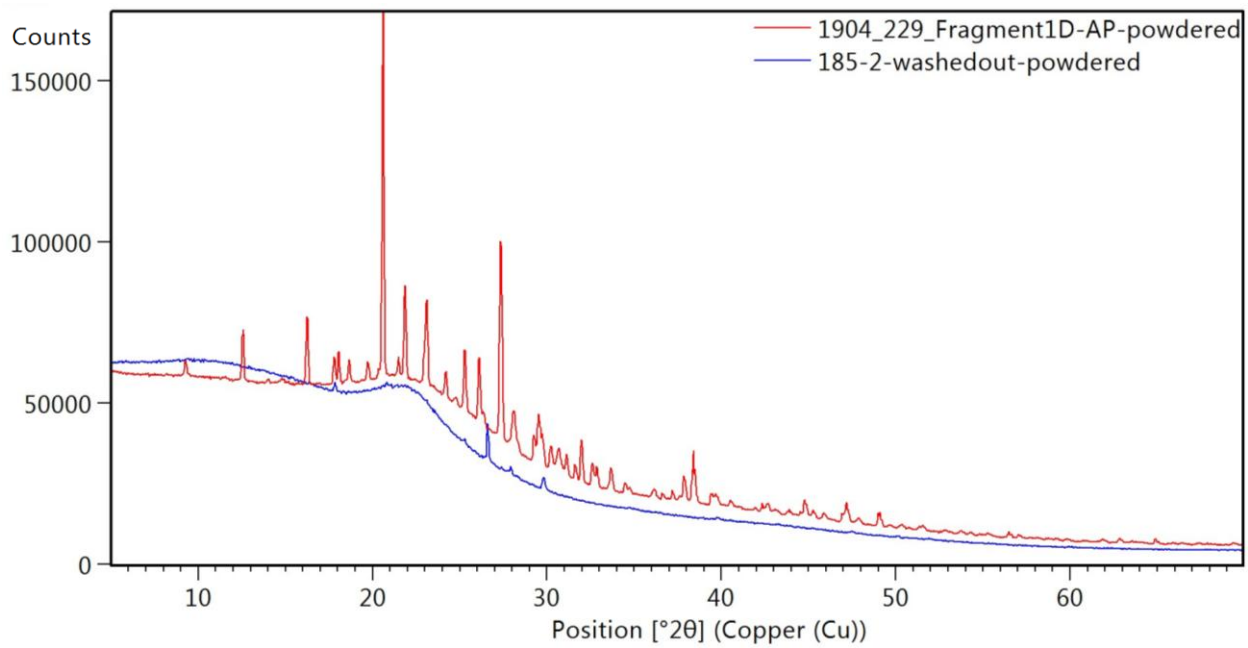

Figure 9: X-ray diffraction pattern obtained for Fragment 1D-AP and remaining wood component of 185-2 after rinsing with water to remove salts.

μFTIR

Though acknowledged as a valuable tool in the characterisation of cultural heritage materials, FTIR microscopy has had limited application to archaeological wood to date. However, the spatial resolution achievable with FTIR microscopy, improved by the use of synchrotron radiation, proved particularly useful for analysis of these inhomogeneous wood samples as a means of identifying compounds present as very small particles. Good quality transmission mode FTIR spectra could thus be obtained from very small spots of the samples, and detailed mapping could be performed. Figure 10 shows a picture of a compressed grain from the 229 fragment 1C-AR under the microscope, on which infrared mapping was performed. The infrared spectra from some points in the map matched the reference spectrum of $KHSO_4$, confirming the results obtained by XRD measurements. $KHSO_4$ was also observed in the spectra from FTIR maps of 1D-AR, 185-6 and 185-3, which in the latter was present in such a small amount relative to alum that it was not seen in the XRD pattern. In these cases, however, the peaks were generally accompanied by significant contributions from alum or the remaining wood.

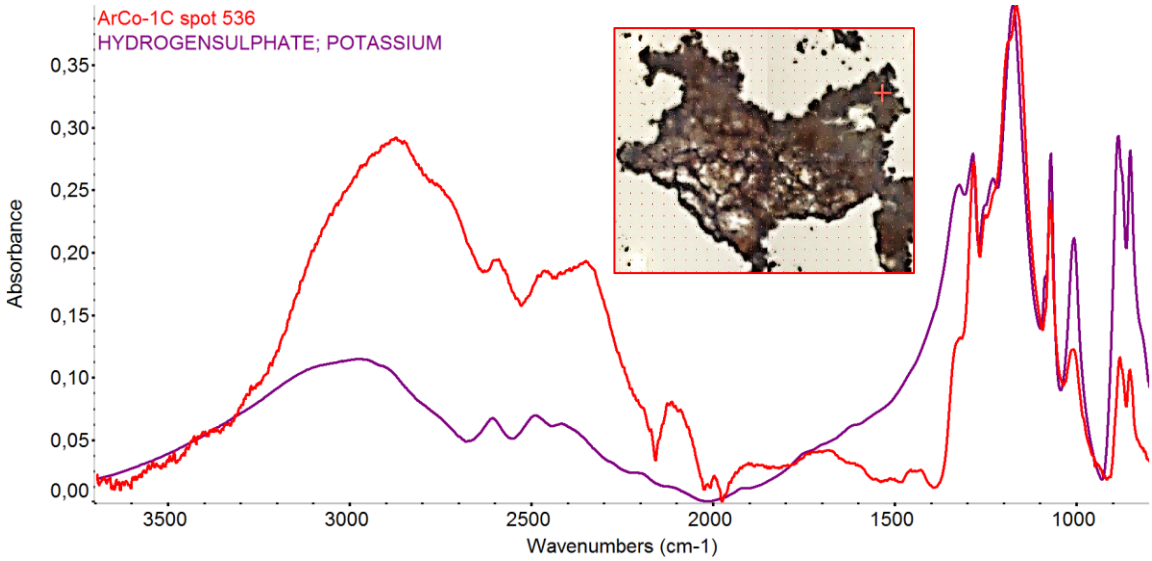

Figure 10: SR μFTIR spectrum of KHSO4 from a point marked with a red cross in the map of a grain from fragment 1C-AR.

Discussion

A large number of analytical techniques were used to investigate both the organic and inorganic components of these particular archaeological wood samples. Therefore, in an attempt to provide an overall interpretation of the data obtained, we aim to highlight correlations between the results provided by the different techniques.

The good agreement between the results obtained by FTIR spectroscopy and Py(HMDS)-GC/MS to evaluate wood degradation allowed us to ease some concerns about the interpretation of the data. It is known that pyrolysis reactions of organic materials can be altered by the presence of inorganic compounds [27, 28]. The occurrence of “pyrolytic artifacts” is a very difficult aspect to consider when interpreting the results obtained from archaeological wood samples. Water-soluble inorganic salts can be in most cases washed out from the samples (as in the case of the 185 series in infrared studies). Nevertheless, especially for highly degraded samples, the washing procedure carries a high risk of removing informative wood degradation products together with

inorganic salts. Therefore, the choice of washing samples or not before pyrolysis is always a very delicate issue. For these samples we decided to perform the analyses without washing. However, in such a case it was impossible to rule out that the high relative abundance of acid lignin pyrolysis products could be partially due to the influence of alum on the formation of secondary wood products during the pyrolysis step. In fact, although no oxygen is present in the pyrolysis chamber, radical oxidation reactions can still occur, producing carbonyl and carboxyl functionalities [29]. However, the clear occurrence of these functional groups in FTIR spectra of the alum-treated samples (Figure 4) was evidence that extensive lignin oxidation had indeed occurred in the unprepared samples of wood and were not artefacts produced by the pyrolysis step. Thus, the Py(HMDS)-GC/MS data actually reflected the composition of the wood.

Similar concerns regarding rinsing samples free from alum prior to infrared spectroscopy should also be noted (Figure 4b). The advantages of obtaining clearer signals from wood after rinsing away alum comes at a cost, due to the simultaneous removal of other compounds, as mentioned above. Thus only major degradation trends in wood may be reliably gleaned from rinsed spectra. Nonetheless, in our case alum-free spectra have enabled an improved understanding of the consequences of the alum treatment on wood. Attempts to 'remove' alum by spectral subtraction still compromised wood signals, giving a spectrum which can be difficult to interpret. Thus, removing alum salt interference in infrared spectra remains a challenge.

In our previous studies of the 185 series [4], we observed some noteworthy correlations between the percentage sum of the acid pyrolysis products, indicative of lignin oxidation, and the concentrations of Al, Fe and Ca obtained by ICP analysis, indicating potential roles of these elements in the extreme degradation of wood. Similar trends and other correlations could be seen in the 229 fragments. Figure 11 shows the variations of Al concentration and the sum of the percentage areas of acid pyrolysis products in these samples.

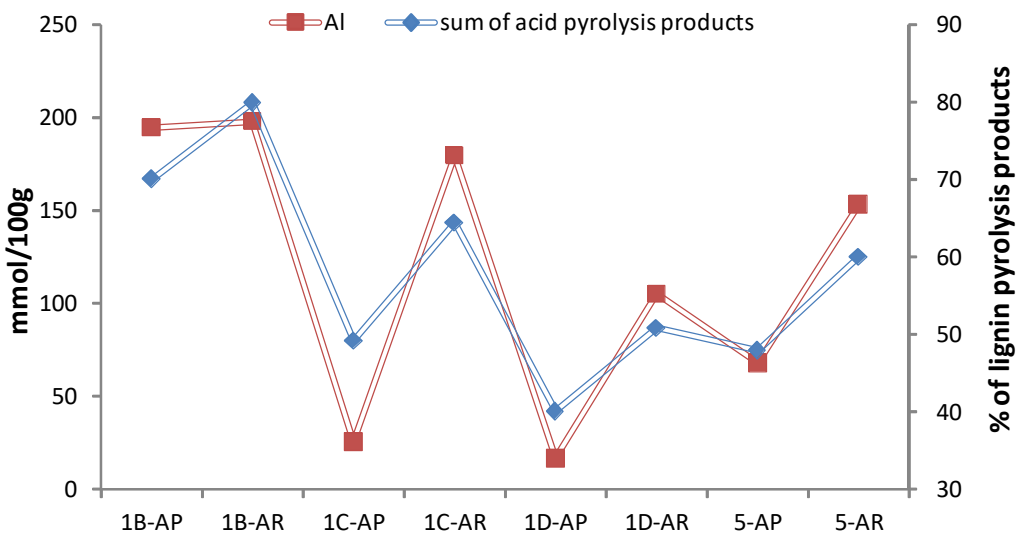

Figure 11: Correlation between the sum of acid lignin pyrolysis products and Al content in the 229 fragments.

The Pearson's *r* correlation index was 0.92, indicating a strong correlation between the two variables. Similar results were obtained comparing the sum of acid pyrolysis products with K and S (r = 0.83 and 0.91, respectively). This supports the previous hypothesis that the extent of lignin oxidation is related to the alum treatment [4].

The correlations with Al and K contents were more evident for the 229 fragments than for the 185 series, while S was not included in the previous analysis. In addition to expected lower contents of Al, K and S in the AP samples with respect to the AR samples, the ICP results also

revealed that the stoichiometric ratios between Al, K and S (Table 1) were variable across the samples. In particular, low values of Al/K and Al/S in 1C-AP and 1D-AP samples suggested that K- and S-containing ions had migrated into the alum-poor regions of these fragments more effectively than Al-containing ions, in agreement with the results obtained by SEM-EDX. In fact, Al was not detected in the 1C-AP and 1D-AP samples by SEM-EDX due to its relatively low concentrations, whereas it was detected in the corresponding AR samples. For the other samples Al/K values were generally close to 1, as they are in alum.

The identification of $KHSO_4$ by both XRD and FTIR analyses in almost all samples is in perfect agreement with these results. In fact, since this mineral does not contain Al, it can provide some explanation of the different distribution of alum-related elements (Al, K and S) in these samples, especially considering that the 229 samples with the lowest Al/K, 1C-AP and 1D-AP (0.4 and 0.3, respectively), were those with the highest relative amount of $KHSO_4$ by XRD. This result was different from that obtained for the 185 series, in which the highest Al/K ratio was 0.2 [4], but a high relative proportion of $KHSO_4$ to alum was not reflected by the XRD patterns. The reason for the low Al/K ratios in these cases remains uncertain even after further inorganic analysis. However, it is apparent that the Al and K contents are more closely associated with the amount of alum in the 229 fragments than in the 185 series, highlighting a significant variability in composition for samples taken from different objects.

The Al/S and K/S values were all lower than the value for alum (Table 1), suggesting that sources of sulphur other than alum are present in the samples. At the same time, IC-LC results suggested that most of the sulphur was present in the form of sulphates. This is consistent with a high level of sulphuric acid being released into the wood during alum treatment, which results from hydrolysis of Al species and is accompanied by the precipitation of aluminium-hydroxide containing compounds, such as alunite ($KAl_3(SO_4)_2(OH)_6$) [3] (Equation 1), the presence of which could account for Al/K ratios higher than 1.

$$3\ KAl(SO_4)_2 + 12\ H_2O \rightarrow KAl_3(SO_4)_2(OH)_6 + 2K^+ + 4\ SO_4^{2-} + 6\ H_3O^+\ [3] \quad \text{(Equation 1)}$$

Given that extremely concentrated solutions of alum were used during treatment, it is likely that some of the K ions released in Equation 1 also precipitated as sulphate salts in the treatment bath such that proportionally more sulphates migrated into the wood than K ions, accompanied by protons in the form of hydronium ions. By assuming the sulphur content reflects the amount of sulphates in the samples, we can estimate the amount of these protons by balancing the charge difference, i.e. for each sulphate dianion not balanced by K^+ or Al^{3+}, we can calculate that the remaining counter-cations are protons (Equation 2). But in cases where [Al] > [K], hydroxide anions may also be present in some species and would interfere with this charge balance. However, by assuming that K is mostly present as alum and alunite in these cases, we can calculate that there are also 2 equivalents of sulphates per K atom in these compounds, and that only the remaining sulphates have protons as counter-ions (Equation 3).

$$[H^+] = 2[S] - 3[Al] - [K] \quad \text{when } [Al] < [K] \quad \text{(Equation 2)}$$
$$[H^+] = 2([S] - 2[K]) \quad \text{when } [Al] > [K] \quad \text{(Equation 3)}$$

Comparing these estimated values to the sum of acid pyrolysis products gave a similar correlation coefficient of 0.92 (Figure 12), very close to that obtained for Al concentration (Figure 11). The estimated H^+ and Al concentrations also correlate strongly with each other (r = 0.94). This could indicate that the apparent correlation between Al and degradation is linked to a relationship between Al and sulphuric acid released from alum decomposition during treatment.

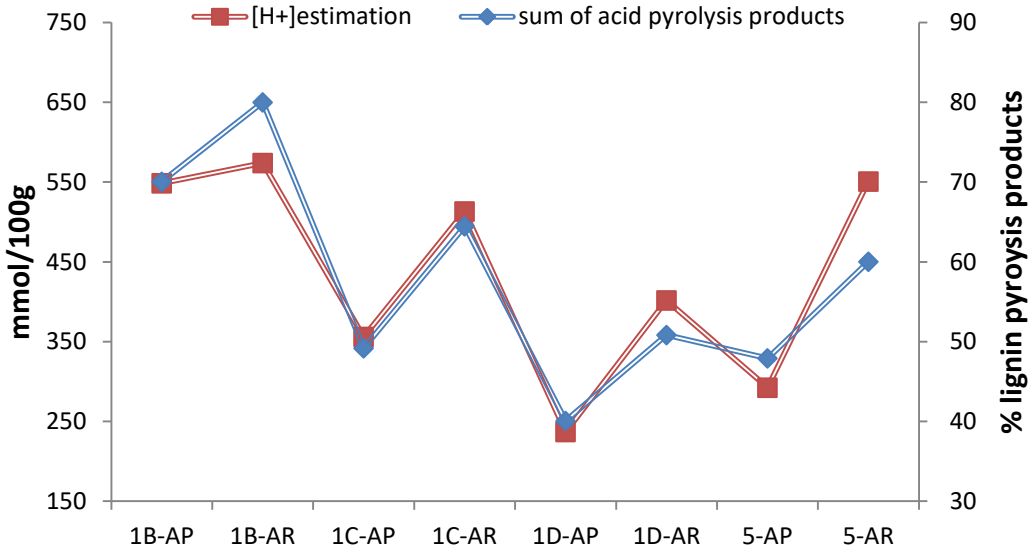

Figure 12: Correlation between sum of acid lignin pyrolysis products with estimation of excess S content not present as alum, alunite or $KHSO_4$

Apart from degrading wood via acid-catalysed hydrolysis, increased acidity can promote iron-catalysed Fenton reactions [30, 31]. In our previous analysis of the 185 series, some correlation between the sum of acid pyrolysis products and iron content was observed, which increased when the difference between concentrations of iron and calcium were considered [4]. In this case, no convincing correlation was found considering the Fe content (r = 0.30), though a notable increase was again observed when the Ca concentration was subtracted from that of Fe (Figure 13), as reflected by an r value of 0.78. This supports the suggestion that a potential modulating effect of calcium compounds on iron-promoted degradation might be worth investigating.

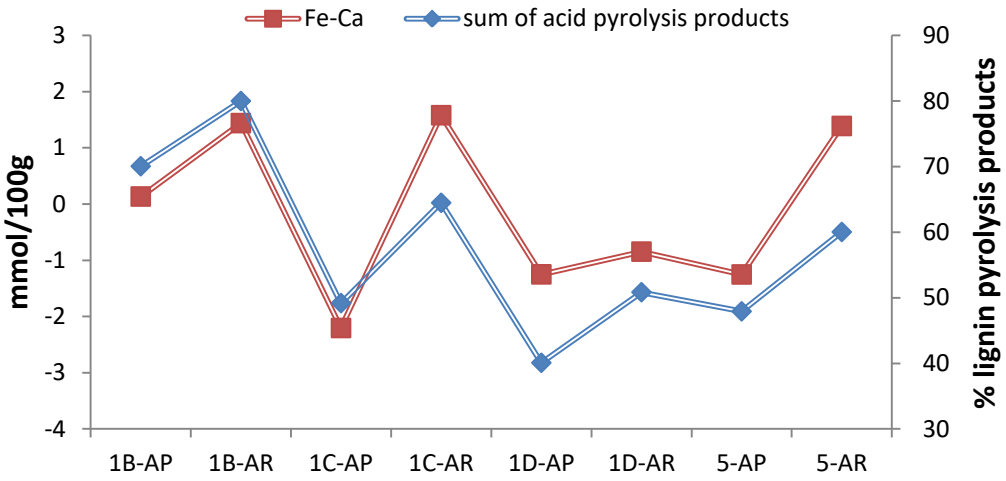

Figure 13: Comparison of the sum of acid lignin pyrolysis products to Fe content minus Ca content in the 229 fragments.

Conclusions

Alum-treated fragments from the Oseberg collection were thoroughly characterised through a range of organic and inorganic analyses. In general, extensive degradation of holocellulose and oxidation of lignin were observed by Py(HMDS)-GC/MS and FTIR spectroscopy, and

morphological studies revealed extreme deterioration of the cell walls. In terms of inorganic components, alum was accompanied by varying amounts of its decomposition product $KHSO_4$ in almost all samples. The ICP, EDX and IC-LC analyses also indicated that there is a large amount of sulphates in all samples not bound as alum or $KHSO_4$, reflecting a high level of sulphuric acid released by hydrolysis of alum during treatment.

One particular aim was to assess differences between the alum-rich surface and alum-poor core regions in the larger fragments. The results obtained by all the techniques for the 229 fragments highlighted that the alum-rich surface samples had a higher extent of wood degradation and a higher inorganic content than the corresponding alum-poor core samples. ICP-OES and SEM-EDX also indicated that K- and S- containing ions had migrated more effectively than Al-ions into the core of the fragments 1C and 1D, which was supported by a larger proportion of $KHSO_4$ relative to alum seen by XRD. The differences in wood degradation correlated with those observed considering the inorganic content. In particular, the percentage sum of acid lignin pyrolysis products correlated strongly with the content of Al, K and S as measured by ICP-OES, as well as an estimation of the acid content, supporting previous suggestions that the extent of wood degradation is directly related to the alum treatment and ensuing release of sulphuric acid. Further work to obtain more accurate measurements of the acid content may therefore be illuminating. Unlike with the 185 series, no convincing relationship between the iron content and wood degradation was observed. However, a good correlation was found considering the subtraction between the concentrations of Fe and Ca, supporting suggestions from a previous study that a potential modulation of iron-promoted degradation by calcium compounds might be worth investigating.

Overall, the results demonstrated a notable variability in the chemical composition of alum-treated fragments from the Oseberg collection, both within the individual fragments and between fragments from the same object. This is something to be taken into account when planning re-treatment strategies; choices of new consolidants, number of retreatment steps, de-acidification strategies might have to be adjusted accordingly. Questions around the chemical stability of the alum in the wood remain, and further work will focus on how this can be assessed. Its removal would certainly be complicated by the extremely compromised wood structure, and future retreatment trials will need to weigh the benefits and drawbacks of combinations of alum removal and de-acidification against each other.

Acknowledgements

This work was carried out as part of two projects: the ArCo project - Ageing Study of Treated Composite Archaeological Waterlogged Artefacts, funded in the framework of JPI - JHEP Joint Pilot Transnational Call for Joint Research Projects on Cultural Heritage, and the Saving Oseberg project, funded by the Norwegian Ministry of Education and University of Oslo. The authors wish to thank Helmholtz-Zentrum Berlin and Paul Scherrer Institute for the allocation of synchrotron beamtime for FTIR and X-ray tomographic measurements respectively. The assistance of Ulrich Schade and Ljiljana Puskar at the IRIS beamline is gratefully acknowledged. The authors also thank Raymund Mokso at the TOMCAT beamline for help with acquisition of X-ray tomographic data and Anders Kæstner, SINQ (at the Paul Scherrer institute) for help with making 3D reconstructions from tomography data.

References

1. Bonde, N. and A.E. Christensen, *Dendrochronological dating ofthe Viking Age ship burials at Oseberg, Gokstad and Tune, Norway.* Antiquity, 1993. **67**: p. 575-583.
2. Brøgger, A.W., H. Shetelig, and H. Falk, *Osebergfundet*. 1917, Oslo: Distribuert ved Universitetets Oldsaksamling. 5 b. : ill.
3. Braovac, S. and H. Kutzke, *The presence of sulfuric acid in alum-conserved wood - Origin and consequences.* Journal of Cultural Heritage, 2012. **13**(3): p. S203–S208.
4. Braovac, S., et al., *Chemical analyses of extremely degraded wood using analytical pyrolysis and inductively coupled plasma atomic emission spectroscopy.* Microchemical Journal, 2016. **124**: p. 368-379.
5. Fors, Y. and S. Magnus, *Sulfur and iron in shipwrecks cause conservation concerns.* Chemical Society Reviews, 2006. **35**: p. 399 - 415.
6. Preston, J., et al., *The effects of Mary Rose conservation treatment on iron oxidation processes and microbial communities contributing to acid production in marine archaeological timbers.* PLoS One, 2014. **9**(2): p. 1-8.
7. Almkvist, G. and I. Persson, *Extraction of iron compounds from wood from the Vasa.* Holzforschung, 2006. **60**: p. 678-684.
8. Almkvist, G. and I. Persson, *Analysis of acids and degradation products related to iron and sulfur in the Swedish warship Vasa.* Holzforschung, 2008. **62**(694-703).
9. Norbakhsh, S., I. Bjurhager, and G. Almkvist, *Impact of iron(II) and oxygen on degradation of oak – modeling of the Vasa wood.* Holzforschung, 2014. **68**: p. 649-655.
10. Dedic, D., et al., *Analysis of lignin and extractives in the oak wood of the 17th century warship Vasa.* Holzforschung, 2014. **68**(4): p. 419-425.
11. Norbakhsh, S., I. Bjurhager, and G. Almkvist, *Mimicking of the strength loss in the Vasa: model experiments with iron-impregnated recent oak.* Holzforschung, 2013. **67**(6): p. 707.
12. Svedström, K., et al., *Structure of oak wood from the Swedish warship Vasa revealed by X-ray scattering and microtomography.* Holzforschung, 2012. **66**: p. 355-363.
13. Almkvist, G. and I. Persson, *Degradation of polyethylene glycol and hemicellulose in the Vasa.* Holzforschung, 2008. **62**: p. 64-70.
14. Hoffmann, P., et al., *The Bremen Cog of 1380 - An electron microscopy study of its degraded wood before and after stabilization with PEG.* Holzforschung, 2004. **58** (3): p. 211-218.
15. Christensen, B.B., *The Conservation of Waterlogged Wood in the National Museum of Denmark :With a report on the methods chosen for the stabilization of the timbers of the viking ships from Roskilde Fjord, and a report on experiments carried out in order to improve upen these methods*. Vol. 1. 1970, Copenhagen: The National Museum of Denmark.
16. Pandey, K.K. and A.J. Pitman, *FTIR studies of the changes in wood chemistry following decay by brown-rot and white-rot fungi.* International Biodeterioration & Biodegradation, 2003. **52**(3): p. 151-160.
17. Schwanninger, M., et al., *Effects of short-time vibratory ball milling on the shape of FT-IR spectra of wood and cellulose.* Vibrational Spectroscopy, 2004. **36**: p. 23–40.
18. Faix , O., *Classification of Lignins from Different Botanical Origins by FT-IR Spectroscopy.* Holzforschung 1991. **45**(s1): p. 21-28.
19. Hesse, M., H. Meier, and B. Zeeh, *Spectroscopy Methods in Organic Chemistry*. 1997, Stuttgart: Georg Thieme.
20. Silverstein, R.M., et al., *Spectrometric Identification of Organic Compounds*. 8th Edition ed. 2014: Wiley.
21. Best, S.P., R.S. Armstrong, and J.K. Beattie, *Infrared metal-ligand vibrations of hexaaquametal (III) ions in alums.* Inorganic Chemistry, 1980. **19**(7): p. 1958-1961.
22. Pandey, K.K., *A study of chemical structure of soft and hardwood and wood polymers by FTIR spectroscopy.* Journal of Applied Polymer Science, 1999. **71**(12): p. 1097-4628.
23. Mohebby, B., *Attenuated total reflection infrared spectroscopy of white-rot decayed beech wood.* International Biodeterioration & Biodegradation, 2005. **55**: p. 247–251.

24. Rodrigues, J., O. Faix, and H. Pereira, *Determination of Lignin Content of Eucalyptus globulus Wood Using FTIR Spectroscopy*, in *Holzforschung - International Journal of the Biology, Chemistry, Physics and Technology of Wood*. 1998. p. 46.
25. Tamburini, D., et al., *Archaeological wood degradation at the site of Biskupin (Poland): wet chemical analysis and evaluation of specific Py-GC/MS profiles.* Journal of Analytical and Applied Pyrolysis, 2015. **115**: p. 7-15.
26. Hutchings, J. *The properties of Alum*. in *Proceedings of the 10th ICOM Group on Wet Organic Archaeological Materials* 2007. Amsterdam: Rijksdienst voor Archeologie, Cultuurlandschap en Monumenten.
27. Carvalho, W.S., et al., *Thermal decomposition profile and product selectivity of analytical pyrolysis of sweet sorghum bagasse: Effect of addition of inorganic salts.* Industrial Crops and Products, 2015. **74**: p. 372-380.
28. Kinata, S.E., et al., *Slow pyrolysis of CCB-treated wood for energy recovery: Influence of chromium, copper and boron on pyrolysis process and optimization.* Journal of Analytical and Applied Pyrolysis, 2013. **104**: p. 210-217.
29. Kotake, T., H. Kawamoto, and S. Saka, *Pyrolysis reactions of coniferyl alcohol as a model of the primary structure formed during lignin pyrolysis.* Journal of Analytical and Applied Pyrolysis, 2013. **104**(0): p. 573-584.
30. Garrido-Ramírez, E.G., B.K.G. Theng, and M.L. Mora, *Clays and oxide minerals as catalysts and nanocatalysts in Fenton-like reactions — A review.* Applied Clay Science, 2010. **47**(3–4): p. 182-192.
31. Henry, W.P., *Non-Enzymatic Iron, Manganese, and Copper Chemistry of Potential Importance in Wood Decay*, in *Wood Deterioration and Preservation*. 2003, American Chemical Society. p. 175-195.